Influence of the Silane Grafting of Polyethylene on the Morphology, Barrier, Thermal, and Rheological Properties of High-Density Polyethylene/Organoclay Nanocomposites

Ali Sharif-Pakdaman, Jalil Morshedian, Yousef Jahani

Department of Polymer Processing, Iran Polymer and Petrochemical Institute, P. O. Box 14965/115, Tehran, Iran

Received 11 July 2011; accepted 14 October 2011
DOI 10.1002/app.36367
Published online 15 January 2012 in Wiley Online Library (wileyonlinelibrary.com).

ABSTRACT: In this work, silane-grafted high-density polyethylene was prepared by reactive extrusion. This product and neat high-density polyethylene were then melt-compounded with organically modified montmorillonite to form nanocomposites. A series of tests, including Fourier transform infrared spectroscopy, small-angle X-ray diffraction, and transmission electron microscopy, were done on the specimens to investigate the grafting efficiency and its compatibilizing effect and the microstructure of the samples. In addition, the thermal, rheological, and barrier properties were examined to study of the grafting effects and nanocomposite characteristics. The results indicate that an intercalated structure could be easily obtained in the nanocomposites with a grafted matrix. A significant reduction in the degree of crystallinity and an increased crystallization temperature with grafting and the incorporation of nanoclay were proven by thermal analysis (differential scanning calorimetry), whereas the melting temperature did not change noticeably. Dynamic rheological testing indicated the disappearance of the Newtonian plateau and solidlike behavior of the nanocomposites based on grafted polyethylene in lower frequencies. Furthermore, the oxygen transfer rate of the samples decreased significantly with the incorporation of nanoclay in the grafted matrix and the moisture crosslinking of the samples. © 2012 Wiley Periodicals, Inc. J Appl Polym Sci 125: E305–E313, 2012

Key words: barrier; compatibilization; nanocomposites; polyethylene (PE)

INTRODUCTION

Because of several advantages, polyethylene (PE) is the most widely used polymer in various applications. PE articles offer a variety of benefits for use in applications in areas such as the packaging industry and containers in comparison to metals and glass. These advantages include flexibility, light weight, low cost, and recyclability. However, the use of neat PE is restricted because of some of its inherent properties, such as a relatively high oxygen and aroma permeability, which weakens the long shelf- life properties required for these applications.[1–21]

In principle, a barrier function can be incorporated into a PE packaging material with alternative technologies, such as the surface treatment of the polymer by fluorination or sulfonation,[2,3,22] multilayer coextrusion (the addition of a layer of barrier material),[1,23,24] or mixing the barrier materials into the base polymer. In the case of PE, the barrier materials usually can be a barrier polymer, such as polyamide or ethylene vinyl alcohol copolymer,[7–11,17–19,25] or a mineral filler, such as talc or mica powder.[12] However, surface treatment technology is not widely used nowadays because of a concern for environmental safety and health. In addition, the coextrusion blow-molding process is generally not available for products with complex shapes and requires specially designed equipment with a substantial capital investment. Therefore, the compounding of PE resin with a good oxygen barrier polymer or platy fillers could be a feasible alternative.

Recently, polymer/clay nanocomposite materials have attracted attention as an alternative route for improving polymer barrierity and other physical and mechanical properties of final products.[13–16,20,21,26–32] Parallel-oriented platelike impermeable clay particles force penetrating gas molecules to wiggle around them in a random walk; hence, the gas diffuses by a tortuous pathway.[14,28] It is well recognized that these superior properties of nanocomposites are due to the dispersion and orientation of clay layers and the extensive delamination of the layered clay structure, which is attributed to the suitable processing conditions and effective interaction of the polymer matrix with the clay surface.[4,15,16,20,27,28,31,33–38]

In the case of polyolefins, because of their nonpolar backbone, naturally hydrophilic clay is immiscible with their hydrophobic polymer matrix. Consequently, modification of the clay surface or/and polymer molecules

Correspondence to: A. Sharif-Pakdaman (a.pakdaman@ippi.ac.ir).

is highly required. The most used compatibilization method is the introduction of a functionalized polymer containing polar groups, such as maleic anhydride grafted or acrylic acid grafted polymers, as a compatibilizer or the use of direct grafting or a functionalizing reaction of the polymer. It has been claimed that these methods can effectively enhance the intercalation of the polymer chain into the clay galleries.[13,15–17,20,26,28,30,33,39–48] The modification of the clay surface is also used for this purpose.[37,44,49,50]

In recent years, a few works have shown that the silane grafting of polyolefins successfully compatibilizes them with montmorillonite (MMT) nanoclay.[42,51–53] It is known that the silanes used in the manufacturing of crosslinkable polyolefins are mainly vinyl silanes, such as vinyltrimethoxysilane (VTMS), which have two functional groups in their chemical structure: one is the C=C group, which can be grafted onto polymer backbones, and the other is ≡Si—OR, which can be hydrolyzed to generate silanols; these groups can be coupled with each other to form crosslinks.[6,52] Therefore, the hydroxyl groups of the silicate layers can react with the alkoxy groups of silane; this causes an improvement in the interfacial adhesion between PE and the clay layers.[53]

In this work, VTMS was used to graft onto PE molecules in reactive extrusion, and the prepared grafted polymers were melt-blended with different levels of nanoclay. As a result, first, we studied the effects of the silane grafting of blow-molding-grade high-density polyethylene (HDPE) on the compatibilization and intercalation of silane-grafted high-density polyethylene (HDPE-*g*-Si)/MMT nanocomposites. Then, effects of clay intercalation and silane grafting on the thermal and rheological properties and oxygen permeability of the nanocomposites was elucidated. We also explain the results about effects of post crosslinking of the prepared nanocomposites (due to the moisture curing of grafted PE) for further enhancement of the barrierity[54,55] and other properties as well as stabilization of the microstructure.

EXPERIMENTAL

Materials

Commercial blow-molding-grade HDPE (BL3), with a melt flow index of 1.2 g/min (5 kg, 190°C) and a density of 0.954 g/cm^3, was received from Jam Petrochemical Co. (Assaluyeh, Iran). VTMS, with the commercial name Silfin-25, was supplied from Evonik (Essen, Germany). Dicumyl peroxide (99%, Concord Co., Taipei, Taiwan) was used as an initiator. Calcium stearate from Merck Co. was used as a processing aid in the melt compounding of nanoclay with grafted PE. Finally, Cloisite 15A, a modified organomontmorillonite (Org-MMT) nanoclay, was purchased from Rockwood Co. (Gonzales, Texas., USA).

Sample preparation

An appropriate amount of dicumyl peroxide (0.1-phr PE) was dissolved in VTMS. This solution was absorbed in PE granules during mixing in a turbo mixer for about 1 h at ambient temperature. From our previous studies[6,56] and also trial and error, we set the optimum amount of VTMS to 4 phr, for which the best melt rheology and silane grafting efficiency were accessible. The enriched PE granules with VTMS and initiator were then fed into a twin-screw extruder (a Brabender plasticorder, Duisburg, Germany; with a length-to-diameter ratio of 45), where the grafting reaction was done. The maximum screw speed was 75 rpm, and the average residence time measured about 2 min. The prepared HDPE-*g*-Si and also neat PE were blended with 2- and 4-phr Org-MMT and again melt-compounded in the twin extruder with a screw speed of 90 rpm. We kept the residence time of mixing constant at 2 min by reducing feeding into the extruder. The temperature profile for both extrusion steps was 145, 160, 170, 180, 185, and 190°C. All of the sample preparations and experiments were done immediately after the extrusions to inhibit moisture crosslinking.

Characterization

Fourier transform infrared (FTIR) studies

FTIR spectra were obtained with an Equinox 55 instrument from Bruker Co. (Ettlingen, Germany). PE-*g*-VTMS samples for spectroscopy analysis were purified from residual VTMS by dissolution in hot refluxing xylene for 6 h, precipitation into acetone, and then drying in vacuum at 80°C for 6 h.[42,52]

X-ray diffraction study

The gallery heights (*d*-spacings) of the neat clay itself and the clay in the HDPE/MMT nanocomposites were measured at room temperature in the transmission mode with small-angle X-ray scattering (SAXS; Hecus, S3-Micro, Graz, Austria) with Cu Kα radiation at a wavelength of 1.542 Å at 50 kV and 1 mA and at a scanning rate of 0.5°/min. The sample-to-detector distance was 263 mm. The test specimens were produced from compression-molding sheets (Dr. Collin press machine, Ebersberg, Germany) with a thickness of 1 mm, and the *d*-spacing of organoclay was computed by the application of Bragg's equation:

$$2d \sin \theta = n\lambda$$

where the variable d is the distance between clay layers, θ and λ are the certain angles and wavelength of incidence respectively, and n is an integer.

Transmission electron microscopy (TEM) analysis

The transmission electron microscope images were obtained from a FEI/Philips EM 208S microscope (Eindhoven, The Netherlands) operating at accelerating voltage of 100 kV to indicate the location of clay particles and the intercalation of polymer molecules in the clay galleries. The clay nanocomposite samples were cut by an ultramicrotome to observe the particles on their edges. Ultramicrotomed slices 30 nm thick and cut with a diamond knife were finally mounted on a copper grid.

Thermal properties

The melting temperature (T_m), crystallization temperature (T_c), heat of fusion (ΔH_f), and heat of crystallization (ΔH_c) of the samples were determined with differential scanning calorimetry (DSC; Netzsch, 200 F3, Selb, Germany). The samples were first heated to 200°C to eliminate their thermal history and subsequently cooled to ambient temperature. The second endotherm was recorded by another heating to 200°C. All scans were carried out at a heating or cooling rate of 10°C/min and under flowing nitrogen. About 5 mg of each sample was placed in a sample pan for each experiment.

Rheological characterization

Dynamic rheological characterizations were carried out on a Rheoplus MCR-300 rheometer (Anton Paar Co., Graz, Austria) in oscillatory mode at a 5% strain (in linear viscoelastic region) with a 25-mm parallel-plate fixture with a gap of 1 mm at 210°C under a nitrogen blanket. The samples used in this study were fabricated in a disk 1 mm in thickness by compression molding. The frequency sweeps were from 0.01 to 600 rad/s.

Permeability analysis

The oxygen permeation rates (P_{O2}'s) of the samples were determined with a gas permeability tester (Brugger, GPD-C, Munich, Germany). The results were recorded as the volume of oxygen permeated from the films on the basis of the pressure difference in the two chambers at a specified time. The test specimens were produced by a cast film (Thermo Haake Rheomix) with a thickness of about 160 μm. These films were cut into circles 15 cm in diameter. The permeation test was carried out at ambient temperature and 35% relative humidity.

Crosslinking and gel content

The samples were exposed to moisture (by their immersion in boiling water for 12 h) whenever the crosslinking required.[52,56] The gel content of samples was measured in agreement with ASTM D 2765-95. Small particles of the samples (ca. 0.3 g) were immersed in refluxed boiling xylene for 16 h. The specimens were then removed, dried, and reweighed. The amount of insoluble material indicated the gel content of each specimen.

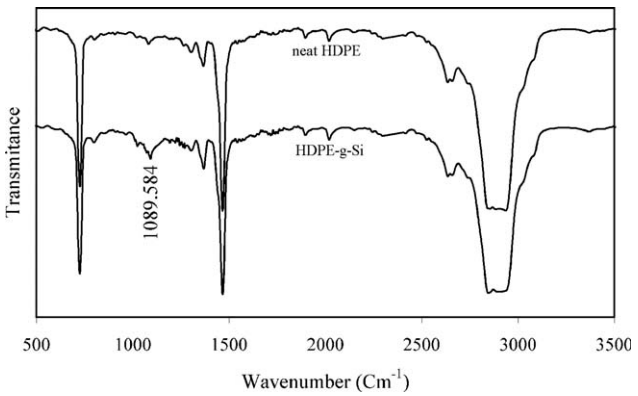

Figure 1 FTIR spectra of neat HDPE and HDPE-*g*-Si with a peak indicated around 1090, which shows Si—OCH_3 groups.

RESULTS AND DISCUSSION

Grafting of VTMS on PE

In the study of the FTIR spectra, the transmittance peaks of interest, which showed the trimethoxysilane groups (Si—OCH_3), were located at wave numbers of 799, 1092, and 1192 cm^{-1}.[57,58] The peak at 1092 cm^{-1} was used as an indication of silane grafting extension in the samples of this study and typically had the strongest absorbance compared to other peaks.[56] Figure 1 shows the transmittance peaks of the neat polymer in comparison with this polymer after the grafting reaction. Obviously, the neat PE had no peaks at the mentioned wave numbers. Therefore, the peak around 1090 cm^{-1} in the grafted samples corresponded to the stretching vibrations of Si—OCH_3 groups and demonstrated the successful grafting reaction on the HDPE molecules. In addition, the increase in the viscosity and the attainment of about 31% gel content after moisture curing confirmed the successful grafting of silane onto the PE backbones.

SAXS and TEM studies

The principle of polymer/clay nanocomposite is based on increasing the gallery space of nanoclay due to the insertion of polymer chains between clay layers; thus, X-ray analysis is a suitable method for evaluating this process.[45] Figure 2 shows the SAXS profiles of the neat clay along with the diffraction spectra of the 2- and 4-phr clay nanocomposites

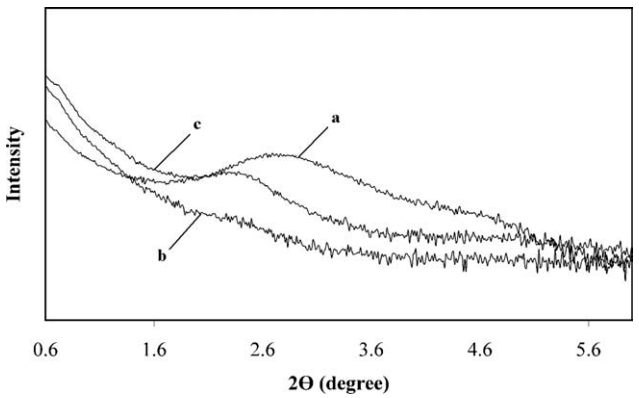

Figure 2 SAXS patterns of (a) MMT, (b) HDPE-*g*-Si (2-phr clay), and (c) HDPE-*g*-Si (4-phr clay).

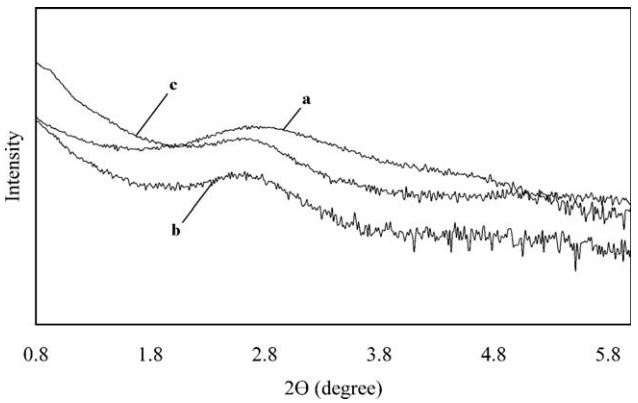

Figure 3 SAXS patterns of (a) MMT, (b) HDPE (2-phr clay), and (c) HDPE (4-phr clay).

with HDPE-*g*-Si. The neat clay (curve a) showed the characteristic peak at a 2θ of around 2.8, which corresponded to a *d*-spacing of 30.35 Å. In both other patterns, the characteristic peak for the clay was shifted to a lower angle, which implied a higher *d*-spacing ($d = 38.4$ Å) according to the Bragg equation ($2d \sin \theta = n\lambda$). This indicated the intercalation of polymer chains inside the clay galleries. There was no distinct shift between the characteristic peaks of curves b and c; this indicated that the intercalation was not affected by a change in the amount of clay in the nanocomposites. However, a decrease in the intensity of diffraction peak b was observed, which corresponded to a lower clay concentration.[37]

Figure 3 repeats the data for the nanocomposites prepared by neat HDPE. As it can be seen obviously, the positions of the characteristic peaks of the neat clay and both of the other nanocomposites did not change significantly, and thus, the nongrafted PE chains did not intercalate efficiently into the clay galleries.

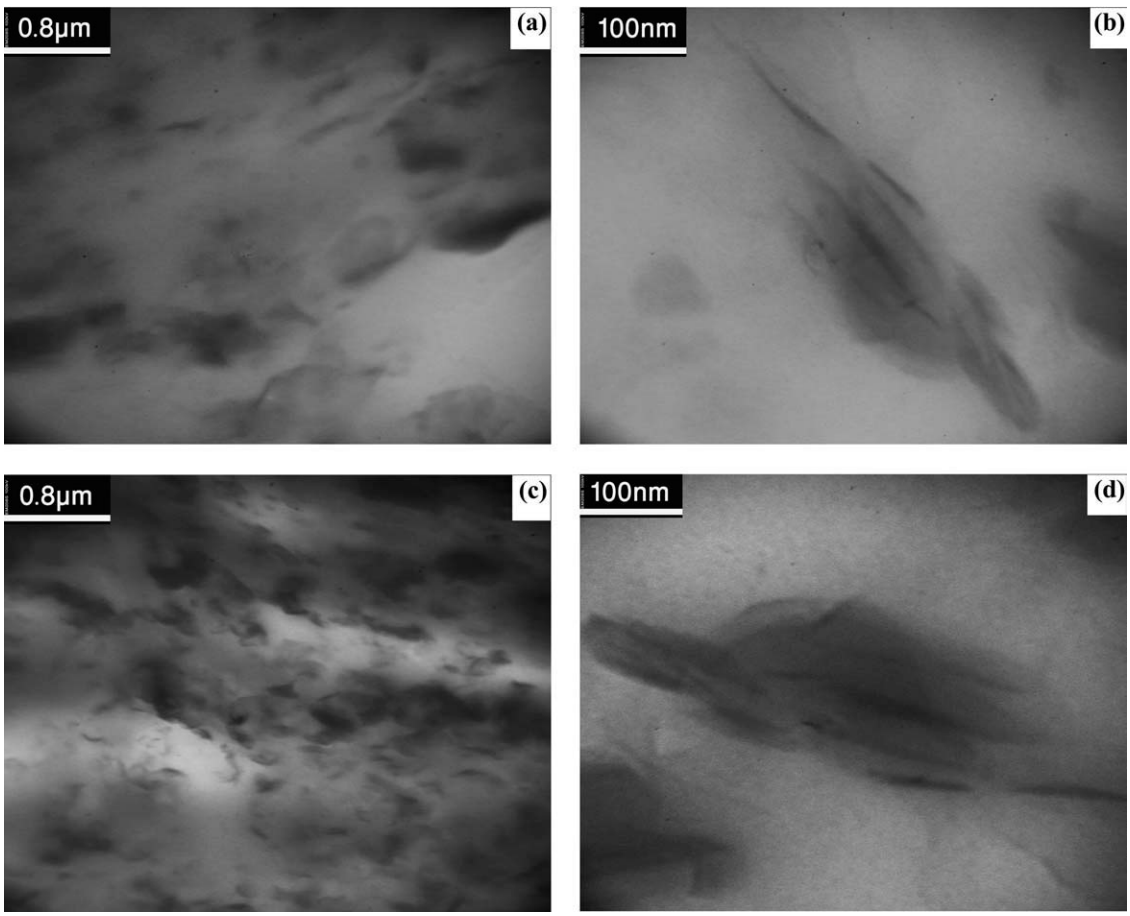

Figure 4 TEM images of the HDPE/clay nanocomposites containing (a,b) 2- and (c,d) 4-phr Org-MMT.

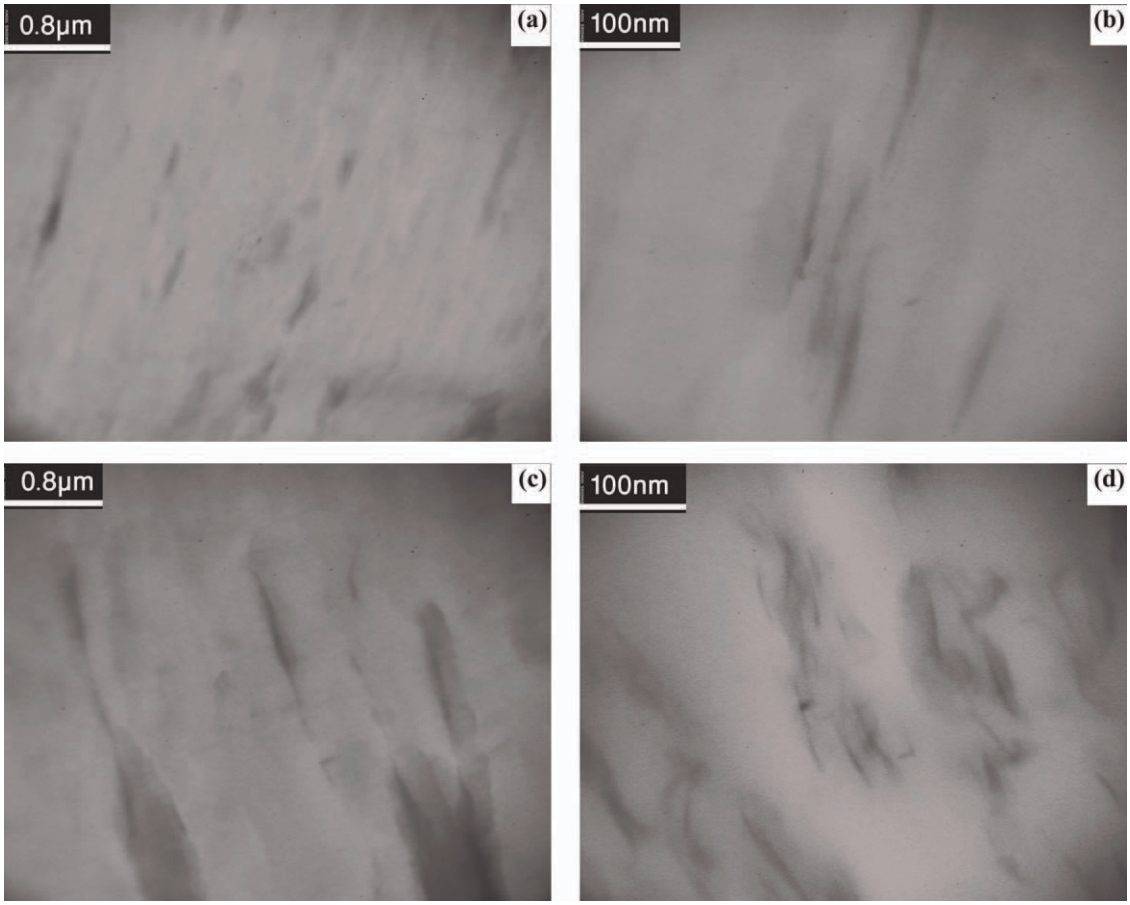

Figure 5 TEM images of HDPE-*g*-Si/clay nanocomposites containing (a,b) 2- and (c,d) 4-phr Org-MMT.

Because X-ray diffraction alone was not enough to determine the nanocomposite morphology, a TEM micrograph was used to directly visualize the dispersion state of the clay layers. Figures 4 and 5 show the TEM images of the nanocomposites with HDPE-*g*-Si and the neat HDPE matrix, respectively, at different magnifications. The black lines and regions represent the clay layer cross sections, and the background represents the polymeric matrix. From Figure 4, it can be seen that a large aggregation of clay was dispersed on the micrometer scale for the HDPE/clay nanocomposites (for samples with both 2- and 4-phr clay) without intercalation and orientation of clay particles. This situation was similar to that of a conventional filled polymer, in which primary particles of a few micrometers are dispersed in the polymer. This result, in agreement with SAXS analysis, showed that the intercalation effect of neat HDPE was limited because of its nonpolar backbone.

The TEM images taken after the silane grafting of PE and shown in Figure 5 revealed that the HDPE-*g*-Si/clay nanocomposites with both 2- and 4-phr clay contents had relatively good dispersion, and an intercalated morphology was visible in most regions. In addition, approximately no agglomeration of clay particles could be observed, especially in samples with 2-phr MMT; this could be attributed to the fact that organoclay had a higher affinity to the more polar grafted HDPE than to neat PE. These finding were in agreement with the SAXS results discussed earlier.

Therefore, the SAXS data and TEM pictures obviously demonstrated that the modification of PE by silane grafting mediated the polarity between HDPE and Org-MMT and had a considerable effect on the compatibilization of HDPE and Org-MMT.[53]

Thermal properties

Figures 6 and 7 show the DSC heating and cooling thermograms of HDPE, HDPE-*g*-Si, the nanocomposites based on neat and grafted PE, and the crosslinked samples. The results of T_m, T_c, ΔH_f, ΔH_c, degree of crystallinity, and gel content of the various mentioned samples are summarized in Table I. The term XLPE in this table related to crosslinked HDPE due to moisture curing of HDPE-*g*-Si.

From Figure 6, it can be seen that all samples exhibited a strong melting peak around 133°C and the T_m of samples did not change considerably by grafting of the matrix or by the incorporation of the nanoclay. Similar results were also reported by

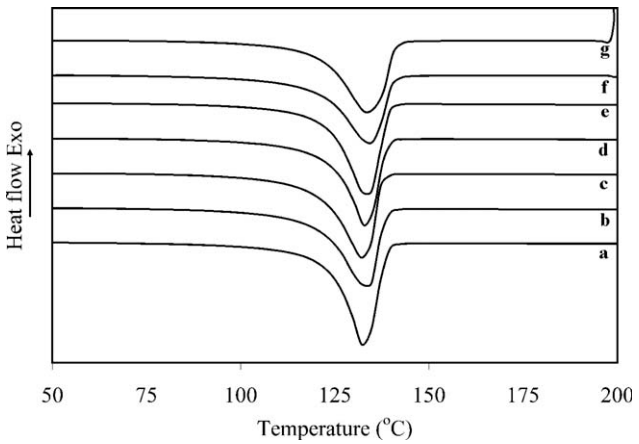

Figure 6 DSC melting endotherms of the samples: (a) HDPE; (b) HDPE/clay, 2 phr; (c) HDPE/clay, 4 phr; (d) HDPE-*g*-Si; (e) crosslinked HDPE; (f) HDPE-*g*-Si/clay, 2 phr; and (g) HDPE-*g*-Si/clay, 4 phr.

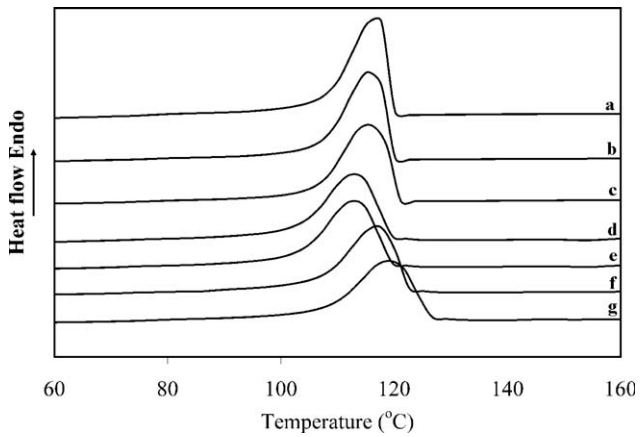

Figure 7 DSC crystallization exotherms of the samples: (a) HDPE, (b) HDPE/clay, 2 phr; (c) HDPE/clay, 4 phr; (d) HDPE-*g*-Si; (e) crosslinked HDPE; (f) HDPE-*g*-Si/clay, 2 phr; and (g) HDPE-*g*-Si/clay, 4 phr.

Bailly and Kontopoulou[42] in the case of polypropylene. It seemed that increasing interactions between the nanoclay and grafted matrix were likely to occur in the amorphous phase and, therefore, did not contribute appreciable changes in the melting behaviors. Furthermore, these results indicate that the addition of nanoclay to both the grafted and neat HDPE did not influence the structure and stability of the PE crystals.

On the other hand, by investigating the cooling behavior (Fig. 7 and Table I), we demonstrated that the addition of organoclay to the neat HDPE also did not produce any significant changes in T_c of HDPE, whereas the nanocomposites produced with grafted HDPE showed a slight increase in T_c. This phenomenon could be related to the increasing surface area available for the nucleation of crystals due to the compatibilization effect of silane grafting.

From Table I, it can be observed that degree of crystallinity, T_c, ΔH_f, and ΔH_c decreased slightly with the silane grafting of PE. Similar results were also obtained for the crosslinked samples. These effects were attributed to the difficulty of crystallization and the decreasing of crystals due to stereo hindrance created by the pendant Si—OCH_3 branches on the HDPE molecules or the increasing amorphous area due to the disability of crosslinked area for crystallization. On the other hand, although the incorporation of nanoclay in the neat HDPE did not show any significant effects on the degree of crystallinity, nanocomposites in the grafted matrices exhibited a considerable decrease in crystallinity compared to their matrix. This trend was perhaps due to a higher interfacial area and adhesion between the PE-*g*-Si and nanoclay; this could have acted to reduce the mobility of crystallizable chain segments. Similar results were reported by Gopakumar et al.[27] for the exfoliation of nanoclay in maleated PE. Finally, an increase in T_c and a further decrease in crystallinity occurred with increasing clay content; this is typical for PE nanocomposites.[27]

Rheological characterization

Dynamic frequency tests were conducted in the linear viscoelastic region (strain = 5%) to further study the microstructure of the nanocomposites and the effect of compatibilization on the rheological parameters. The storage modulus (G'), complex viscosity (η^*), and loss tangent (tan δ) of the samples as a function of angular frequency (ω) are shown in Figure 8(a–c), respectively.

Figure 8(a) shows that in neat PE and their nanocomposites, G' increased monotonically with increasing frequency; and no significant difference in G' was observed between these samples. These results

TABLE I
Thermal Properties of the Samples

Sample	T_m (°C)	ΔH_f (J/g)	T_c (°C)	ΔH_c (J/g)	Crystallinity (%)	Gel content (%)
HDPE	133.3	182.6	116.8	181.9	62.2	0.12
HDPE-*g*-Si	132.6	175.6	114.9	172.5	59.8	4.3
HDPE/clay 100/2	133.5	180.8	116.3	185.4	61.6	—
HDPE/clay 100/4	133.1	179.4	117.1	181.0	61.2	—
HDPE-*g*-Si/clay 100/2	132.8	160.9	119.1	159.3	54.8	—
HDPE-*g*-Si/clay 100/4	132.4	157.1	119.9	158.7	53.5	—
XLPE	132.1	174.7	115.0	173.2	59.5	31

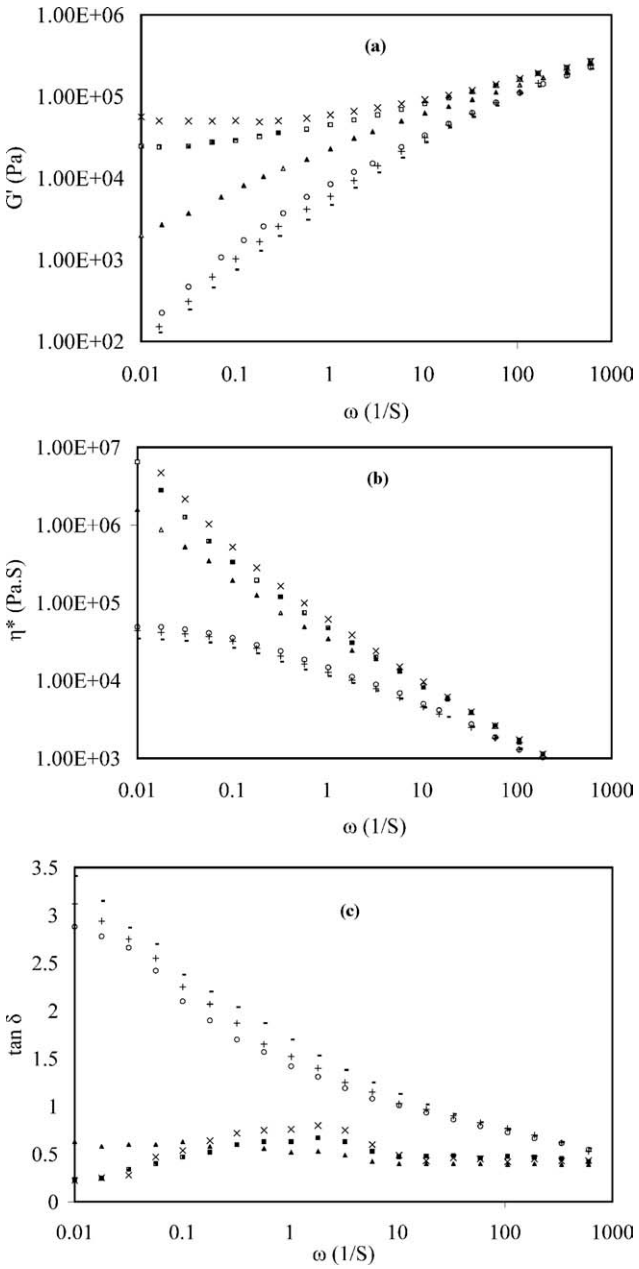

Figure 8 (a) Storage modulus (b) Complex viscosity, and (c) loss tangent of samples as a function of frequency. Symbols are (—) HDPE; (▲) HDPE-*g*-Si; (■) HDPE-*g*-Si/clay 2 phr; (×) HDPE-*g*-Si/clay 4 phr; (+) HDPE/clay 2 phr; (○) HDPE/clay 4 phr.

imply that there was no interaction between the clay layers and HDPE chains without compatibilization. Furthermore, a small increase occurring in G' of the nanocomposite samples relative to HDPE at low frequencies could be just defined as a filler effect due to the dispersion of the nanoclay on the microscale. In addition, a significant increase in G' of the silane-grafted PE could be seen; however, the frequency dependence was not altered considerably. This trend could be attributed to the structural change of PE and the presence of partially crosslinked regions created during the grafting reaction and sample preparation.

On the other hand, the G' values of the HDPE-*g*-Si nanocomposites were the highest in the entire range of frequency studied; this behavior was obtained especially in the low-frequency region. In addition, it was observed that at lower frequencies, G' exhibited a diminished frequency dependence for these nanocomposites. This is characteristic behavior of solidlike materials. The low-frequency improvement and solidlike behavior of G' were due to physical network formation of the clay layers and polymer chains; this indicated strong interactions between the nanoclay and polymer matrix and has been reported for LLDPE/clay nanocomposite systems as well.[15,16]

As shown from the results in Figure 8(b), HDPE and nanocomposites based on neat PE showed a Newtonian plateau in the η* versus ω curve at low-frequency regions; whereas the Newtonian plateau disappeared in the grafted HDPE and related nanocomposites. Therefore, the viscosity curves in the low-frequency region could be fitted by the power law model. Moreover, the viscosity increased dramatically with the grafting of HDPE at low frequencies; this is ordinary for silane-grafted PE.[6] However, the increase in η* with the incorporation of nanoclay into the grafted matrix was more considerable than that in HDPE. These results again confirmed the effect of silane grafting on the interfacial interactions and clay dispersion in the polymer phase.

However, the grafted samples exhibited shear thinning behaviors, Further investigation was done on the slope of log η* versus log ω [Fig. 8(b)] at low frequencies according to the power law model that corresponded to the shear thinning exponent (n):

$$|\eta^*| = k\omega^n$$
$$\mathrm{Log}|\eta^*| = \log k + n \log \omega$$

where, k is a sample specific pre-exponential factor.

The power law exponent (n) could be directly obtained from the slope of the straight line of the curves at low frequencies. This parameter for our samples is listed in Table II. It is seen that n values of the nanocomposites based on grafted HDPE experienced higher changes than other composites. Therefore, it could be expected that HDPE-*g*-Si would yield better clay dispersion in the polymer matrix.[15]

TABLE II
Shear Thinning Exponents of the Samples

Sample	$-n$
HDPE	0.087
HDPE-*g*-Si	0.774
HDPE/clay 100/2	0.095
HDPE/clay 100/4	0.094
HDPE-*g*-Si/clay 100/2	0.852
HDPE-*g*-Si/clay 100/4	0.861

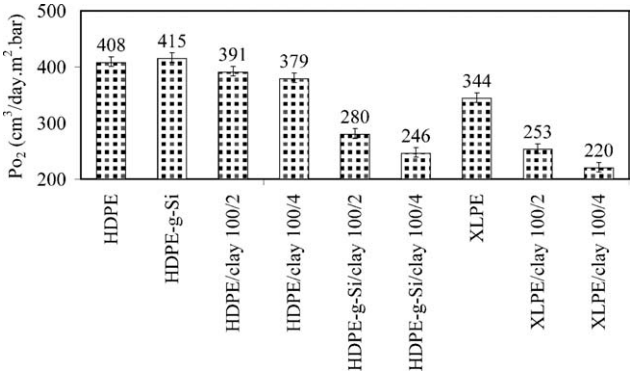

Figure 9 Oxygen permeability of the HDPE, HDPE-*g*-Si, crosslinked HDPE, and their relative nanocomposites.

Similarly, the variation of tan δ versus frequency [Fig. 8(c)] for the grafted samples and nanocomposites showed solidlike behavior (tan $\delta < 1$) in all regions, whereas the neat HDPE and relative nanocomposites had a negative slope in their curve. This was attributed to typical behavior of a viscoelastic liquid. Moreover, the elastic behavior (positive slope) could only be seen at low frequencies in the HDPE-*g*-Si nanocomposites.

Finally, by investigation of Figure 8(a,b), it is obviously demonstrated that the viscoelastic behavior at high frequencies was approximately unaffected by the addition of organoclay. This result was perhaps due to weak physical bonding between the nanoclay and the matrix, even in the grafted samples, which was demolished at higher frequencies.

Permeability analysis

In the case of PE nanocomposites, an improvement in the barrier properties is one of the most fundamental consequences of heavy use in packaging industries. The P_{O2} values of our samples are illustrated in the bar chart of Figure 9. P_{O2} in this chart presents the cubic centimeters of oxygen permeate per square meter of film surface in 1 day (cm^3 day^{-1} m^{-2} bar^{-1}).

Interestingly, the silane-grafted films showed the worst oxygen barrier properties of these samples so that oxygen permeated from the grafted PE about 1.7% more than did neat HDPE. Because it is generally recognized that permeant molecules can only permeate through noncrystalline regions, this effect may have been due to an increase in the amorphous region by the grafting of the PE chains. Unlike the nanocomposites based on the HDPE matrix, which showed a small enhancement in barrierity, the incorporation of the nanoclay in the grafted HDPE showed a considerable effect on the barrierity of samples. The permeation rates of oxygen decreased by 31.4 and 39.8% for the nanocomposites based on HDPE-*g*-Si with 2- and 4-phr nanoclay, respectively. Because the crystallinity almost decreased with the incorporation of nanoclay in the polymer matrix (see Table I), the barrierity enhancement was ascribed to the better dispersion and intercalation of clay particles, which created a more tortuous path for the diffusion in the amorphous regions and a reduction in the chain mobility of the polymer by high interaction between the nanoclay and grafted samples. Furthermore, the results clearly demonstrate that the grafted samples indicated further barrierity enhancement after moisture curing (also see Table I for the gel content data). The grafted samples showed a 17% reduction in the permeability after exposure to moisture (crosslinking). Similarly, the nanocomposites with a grafted matrix yielded better barrierity after crosslinking. This effect was explained by a reduction in the chain mobility of the polymer as a result of crosslinking in the amorphous regions and was reported by Sodergard et al.[55]

CONCLUSIONS

The preparation, characterization, and microstructure of nanocomposites based on HDPE-*g*-Si have been reported. Nanocomposites were prepared from the melt blending of HDPE-*g*-Si or neat HDPE with organoclay. It was shown that silane grafting facilitated the dispersion of nanoclay in the matrix, and grafted polymer chains were successfully intercalated into the nanoclay layers. It was also demonstrated that the resulting thermal, rheological, and barrier properties were sensitive to the composite structure and grafting.

Thermal analysis showed that T_m of the samples did not change considerably by grafting of the matrix or by the incorporation of nanoclay. On the other hand, the nanocomposites produced with grafted HDPE showed a slight increase in T_c; this could have been related to the increasing surface area available for the nucleation of crystals due to compatibilization effect of silane grafting. In addition, although the incorporation of nanoclay in neat HDPE did not show any significant effect on the degree of crystallinity, nanocomposites in the grafted polymers showed a relatively considerable decrease in crystallinity compared to their matrix.

From dynamic frequency tests, we concluded that the G' values of the HDPE-*g*-Si nanocomposites were the highest at lower frequencies, and also, G' exhibited a diminished frequency dependence for these nanocomposites, which is a characteristic behavior of solidlike materials. On the other hand, HDPE and nanocomposites based on neat PE showed a Newtonian plateau in the η^* versus ω curve in the low-frequency region, whereas this plateau disappeared in the grafted HDPE and related nanocomposites so that the viscosity curves in the low-frequency

region could be fitted by the power law model. These observations confirmed increased interactions between the nanoclay and grafted PE.

Although the nanocomposites based on the HDPE matrix showed a small enhancement in barrierity, the incorporation of nanoclay in the grafted HDPE showed a considerable effect on the barrierity of the samples. Interestingly, we found that the grafted samples indicated further barrierity enhancement after moisture curing. Similarly, nanocomposites with a grafted matrix yielded better barrierity after crosslinking.

Finally, we concluded that silane grafting is an economical and easily accessible method for the compatibilization of HDPE and nanoclay, which in addition to the modification of rheological behavior and the structure of nanocomposites, have an advantage of moisture crosslinkability for further enhancement of barrierity and stabilization of microstructure.

References

1. Lange, J.; Wyser, Y. Packag Technol Sci 2003, 16, 149.
2. Sabne, M. B.; Thombre, S. M.; Patil, A. S.; Patil, S. D.; Idage, S. B.; Vernekar, S. P. J Appl Polym Sci 1995, 58, 1275.
3. Serpe, G.; Huiban, Y.; Lynch, J.; Dole-Robbe, J. P.; Legeay, G. J Appl Polym Sci 1996, 61, 1707.
4. Kamal, M. R.; Garmabi, H.; Hozhabr, S.; Arghyris, L. Polym Eng Sci 1995, 35, 41.
5. Yeh, J. T.; Fan-Chiang, C. C.; Yang, S. S. J Appl Polym Sci 1997, 64, 1531.
6. Morshedian, J.; Mohammad-Hoseinpour, P. Iranian Polym J 2009, 18, 103.
7. Yeh, J. T.; Jyan, C. F.; Yang, S. S.; Chou, S. Polym Eng Sci 1999, 39, 1952.
8. Lee, S. Y.; Kim, S. C. Polym Eng Sci 1997, 37, 463.
9. Park, S. H.; Lee, G. J.; Im, S. S. Polym Eng Sci 1998, 38, 1420.
10. Wang, Q.; Qi, R.; Shen, Y.; Lio, Q.; Zhou, C. J Appl Polym Sci 2007, 106, 3220.
11. Chatreenuwat, B.; Nithitanakul, M.; Grady, B. P. J Appl Polym Sci 2007, 103, 3871.
12. Gill, T. S.; Xanthos, M. J Vinyl Additive Technol 1996, 2, 248.
13. Jacquelot, E.; Espuche, E.; Gerard, J. F.; Duchet, J.; Mazabraud, P. J Polym Sci Part B 2006, 44, 431.
14. Choudalakis, G.; Gotsis, A. D. Eur Polym J 2009, 45, 967.
15. Durmus, A.; Kasgoz, A.; Macosko, C. W. Polymer 207, 48, 4492.
16. Durmus, A.; Maybelle, W.; Kasgoz, A.; Macosko, C. W.; Tsapatsis, M. Eur Polym J 2007, 43, 3737.
17. Faisant, J. B.; Ait-Kadi, A.; Bousmina, M.; Deschenes, L. Polymer 1998, 39, 533.
18. Yeh, J. T.; Huang, S. S.; Chen, H. Y. Polym Eng Sci 2005, 45, 25.
19. Yeh, J. T.; Huang, S. S.; Yao, W. H.; Wang, I. J.; Chen, C. C. J Appl Polym Sci 2004, 92, 2528.
20. Ranade, A.; Nayak, K.; Fairbrother, D.; D'souza, N. A. Polymer 2005. 46, 7323.
21. Erdmann, E.; Acosta, D.; Pita, V. J. R. R.; Monasterio, F. E.; Carrera, M. C.; Dias, M. L.; Destefanis, H. A. J Appl Polym Sci 2010, 118, 2467.
22. Kharitonov, A. P. Chem Sustainable Dev 2004, 12, 625.
23. Schut, J. H. Plast Technol 1992, 5, 52.
24. Chandramoul, K.; Jabarian, S. A. Adv Polym Technol 1995, 14, 35.
25. Yeh, J. T.; Yao, W. H.; Du, Q.; Chen, C. C. J Polym Sci Part B 2005, 43, 511.
26. Wang, K. W.; Choi, M. H.; Chung, I. J.; Choi, Y. S. Polymer 2001, 42, 9819.
27. Gopakumar, T. G.; Lee, J. A.; Kontopoulou, M.; Parent, J. S. Polymer 2002, 43, 5483.
28. Osman, M. A.; Rupp, J. E. P. Macromol Rapid Commun 2005, 26, 880.
29. Sorrentino, A.; Tortora, M.; Vittoria, V. J Polym Sci Part B 2006, 44, 265.
30. Picard, E.; Vermogen, A.; Gerard, J. F.; Espuche, E. J Membr Sci 2007, 292, 133.
31. Mederic, P.; Razafinimaro, T.; Aubry, T.; Moan, M.; Klopffer, M. H. Macromol Symp 2005, 221, 75.
32. Frounchi, M.; Dadbin, S.; Salehpour, Z.; Noferesti, M. J Membr Sci 2006, 282, 142.
33. Qi, R.; Jin, X.; Zhou, C. J Appl Polym Sci 2006, 102, 4921.
34. Artezi, N.; Narkisi, M.; Siegmann, A. Polym Eng Sci 2004, 44, 1019.
35. Osman, M. A.; Rupp, J. E. P.; Suter, U. W. Polymer 2005, 46, 1653.
36. Zhong, Y.; Kee, D. D. Polym Eng Sci 2005, 45, 469.
37. Chu, D.; Nguyen, Q.; Baird, D. G. Polym Compos 2007, 28, 499.
38. Lee, S. Y.; Kim, S. C. J Appl Polym Sci 1998, 67, 2001.
39. Conteras, V.; Cafiero, M.; Da Silva, S.; Rosales, C.; Perera, R.; Matos, M. Polym Eng Sci 2006, 46, 1111.
40. Kusmono; Mohd Ishak, Z. A.; Chow, W. S.; Takeichi, T.; Rochmadi. Eur Polym J 2008, 44, 1023.
41. Fang, Z.; Xu, Y.; Tong, L. Polym Eng Sci 2007, 47, 551.
42. Bailly, M.; Kontopoulou, M. Polymer 2009, 50, 2472.
43. Valdez, S. S.; Nonell, J. M.; Rodriguez, F. J. M.; Vargas, E. R.; Colunga, J. G. M.; Valdez, H. S.; Jimenez, L. M.; Velazquez, G. N. Polym Bull 2009, 63, 921.
44. Yazdani, H.; Morshedian, J.; Khonakdar, H. A. Polym Compos 2006, 27, 491.
45. Paul, D. R.; Robeson, L. M. Polymer 2008, 49, 3187.
46. Filippi, S.; Chiono, V.; Polacco, G.; Paci, M.; Minkova, L. I.; Magagnini, P. Macromol Chem Phys 2002, 203, 1512.
47. Fillipi, S.; Dintcheva, N. T.; Scaffaro, R.; La Manita, F. P.; Polacco, G.; Magagnini, P. Polym Eng Sci 2009, 49, 1187.
48. Dayma, N.; Satapathy, A. A. Mater Des 2010, 31, 4693.
49. Qian, Z.; Zhou, H.; Xu, X.; Ding, Y.; Zhang, S.; Yang, M. Polym Compos 2009, 30, 1234.
50. Scaffaro, R.; Misteretta, M. C.; La Manita, F. P. Polym Degrad Stab 2008, 93, 1267.
51. Nachtigall, S. M. B.; Felix, A. H. O.; Mauler, R. S. J Appl Polym Sci 2003, 88, 2492.
52. Lu, H.; Hu, Y.; Li, M.; Chen, Z.; Fan, W. Compos Sci Technol 2006, 66, 3035.
53. Wang, H.; Fang, P.; Chen, Z.; Wang, S.; Xu, Y.; Fang, Z. Polym Int 2008, 57, 50.
54. Raj, B.; Jagadish, R. S.; Srinivas, P.;Siddaramaiah. J Appl Polym Sci 2005, 96, 1193.
55. Sodergard, A.; Ekman, K.; Stenlund, B.; Lassas, A. C. J Appl Polym Sci 1996, 59, 1709.
56. Morshedian, J.; Mohammad-Hoseinpour, P.; Azizi, H.; Parvizzad, R. Express Polym Lett 2009, 3, 105.
57. Hjertberg, T.; Palmlof, M.; Sultan, B. A. J Appl Polym Sci 1991, 42, 1185.
58. Mallegol, J.; Carlsson, D. J.; Deschenes, L. Polym Degrad Stab 2001, 73, 259.